KSCE Journal of Civil Engineering (2022) 26(3):1095-1110
DOI 10.1007/s12205-021-1162-y

pISSN 1226-7988, eISSN 1976-3808
www.springer.com/12205

Geotechnical Engineering

Investigations of Silty Soil Slopes under Unsaturated Conditions Based on Strength Reduction Finite Element and Limit Analysis

An-Jui Li[a], Joram Wachira Mburu[a], Chao Wei Chen[b], and Kuo-Hsin Yang[c]

[a]*Dept. of Civil and Construction Engineering, National Taiwan University of Science and Technology, Taipei 10607, Taiwan*
[b]*Land Engineering Consultants Co., Ltd., Taipei 115020, Taiwan*
[c]*Dept. of Civil Engineering, National Taiwan University, Taipei 10617, Taiwan*

ARTICLE HISTORY

Received 28 June 2021
Revised 22 September 2021
Accepted 4 October 2021
Published Online 7 December 2021

KEYWORDS

Apparent cohesion
Matric suction
Stability chart
Strength reduction
Landslide

ABSTRACT

Matric suction plays a key role in slope stability by conferring an apparent cohesion component to the unsaturated portion of the soil. This paper adopts the total cohesion method to investigate the contribution of apparent cohesion on the stability of silty slopes under hydrostatic conditions. Phase^2 and Optum G2 numerical programs, based on strength reduction finite element analysis and finite element limit analysis methods, respectively, are used for numerical analysis. Generally, Phase^2 and Optum G2 results are in good agreement with each other. Optum G2 yields slightly higher factor of safety results than Phase^2, particularly for steep slopes $\beta \geq 30^\circ$. The results are presented in form of stability charts which are validated with a case from a previous study. Notably, the contribution of apparent cohesion to unsaturated shear strength is most pronounced when varying the water table. An examination of the slope failure mechanism reveals that the toe failure mechanism is the dominant failure mechanism. The depth of the failure surface is most sensitive to changes in the slope angle, cohesion and water table position. The influence of the air-entry value on the depth of the failure surface is contingent upon the location of the water table.

1. Introduction

Landslides occur throughout the world under different climatic conditions and terrain resulting in economic disruption, displacement of people and loss of lives. Growing populations, limited in geographic expansion, may occupy unstable, steep or remote areas. For example, significant economic growth and urbanization in Northern Taiwan has translated to increase in land development and construction on unsaturated soil slopes (Lin et al., 2016). This coupled with storm-induced landslides particularly in tropical and subtropical climatic regions, such as Taiwan, Hong Kong, Singapore, and Japan have increased attention given to slope stability problems (Brand, 1984; Fourie, 1996).

Silty soil is susceptible to water erosion particularly in areas with high rainfall and sloping grounds (Finch et al., 2014). This explains why slope failures involving silty slopes is quite common in East and South Asia region which is defined by heavy rainfall and sloping mountain ranges (Oguchi et al., 2011; Yang et al., 2021). Past studies have focused on individual case studies which cover a limited range of soil and slope parameters. There is still need of a more comprehensive study which incorporates a wider range of soil and slope properties.

Traditional slope stability assessments did not consider unsaturated slope conditions by assuming the groundwater rises to the surface as a worst case scenario, neglecting negative pore water pressures. As much as this is a more conservative approach, it may lead to overdesigning and underestimating the stability of a slope. An actual case study on two Hong Kong cut slopes by Ching et al. (1984) revealed that computed factors of safety without considering suction were unreasonably low. Inclusion of matric suction in stability analysis yielded about 17% and 20% increase in factor of safety respectively for the two slopes.

Additionally, Rahardjo et al. (1995) also demonstrated the importance of matric suction with regards to the stability of residual slopes in Singapore, stating that slip surfaces associated with shallow landslides mostly occur above the water table, necessitating the estimation of negative pore water pressures. Oloo et al. (1997) noted that matric suction might possibly have

CORRESPONDENCE Joram Wachira Mburu d10805812@mail.ntust.edu.tw Dept. of Civil and Construction Engineering, National Taiwan University of Science and Technology, Taipei 10607, Taiwan

a significant effect on the bearing capacity of thin pavement structures. Similarly, Rassam and Williams (1999) showed that the stability of tailing dams increased by about 30% when matric suction was incorporated in slope stability analysis. Chae et al. (2010) studied the relationship between matric suction and undrained shear strength using unconfined compression tests on silty soils. More recently, Ng et al. (2013), Han and Vanapalli (2016) and Yao et al. (2018) investigated the effect of matric suction on resilient modulus of unsaturated subgrade soils. Pang and Gu (2020) studied the effect of apparent cohesion in 3D non-homogeneous, unsaturated slopes under steady flow.

This study investigates the contribution of apparent cohesion to the stability of silty slopes under hydrostatic conditions covering a wide range of soil and slope parameters. Different soil and slope conditions are identified where apparent cohesion can be considered or ignored. The Phase^2 and Optum G2 software are used for numerical analysis. The results, conveniently presented in form of stability charts similar to Michalowski (2002) and Li et al. (2010), clearly demonstrate the effect of unsaturated conditions on slope stability. The failure surfaces generated under different slope and soil conditions through maximum shear strain contour plots are also examined and discussed.

2. Theoretical Background

Fredlund et al. (1978) extended the typical two-dimensional Mohr Coulomb model plot to a three-dimensional plot to cater for unsaturated soils, the third dimension being matric suction. The shear strength equation for unsaturated soil is shown in Eq. (1) as follows:

$$\tau_{ff} = c' + (\sigma_f - u_a)_f \tan\phi' + (u_a - u_w)_f \tan\phi^b, \quad (1)$$

where c' = Effective cohesion (intercept of extended Mohr Coulomb failure envelope on shear stress axis where the net normal stress and matric suction are equal to zero), $(\sigma_f - u_a)_f$ = net normal stress state on the failure plane at failure, $(u_a)_f$ = pore-air pressure on the failure plane at failure, ϕ' = angle of internal friction associated with the net normal stress state variable, $(\sigma_f - u_a)_f$, $(u_a - u_w)_f$ = matric suction on the failure plane at failure, and ϕ^b = angle indicating the rate of increase in shear strength with respect to a change in matric suction, $(u_a - u_w)_f$.

The inclusion of matric suction as a third dimension to the Mohr-Coulomb model introduces a suction component of the shear strength which is known as the apparent cohesion. This is denoted as $(u_a - u_w)_f \tan\phi^b$. The effects of matric suction can be evaluated using apparent cohesion. When added to the effective cohesion, c', the total cohesion, c is obtained as shown in Eq. (2) below (Fredlund et al., 2012):

$$c = c' + (u_a - u_w)_f \tan\phi^b, \quad (2)$$

where c = intercept of the extended Mohr-Coulomb failure envelope with shear stress at a particular matric suction $(u_a - u_w)_f$. This is referred to as total cohesion at zero net normal stress.

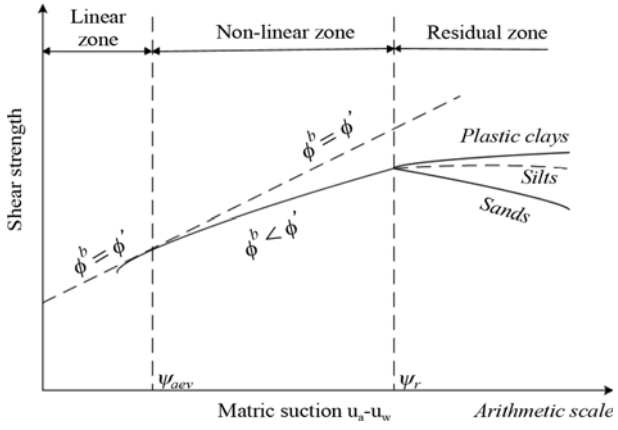

Fig. 1. Typical Unsaturated Shear Strength Envelopes (Zhang et al., 2014)

The soil water characteristic curve (SWCC) gives the likely range of suction to be encountered in the field and water retention capability of soil. The SWCC shape is mainly determined by the grain size distribution and can be developed from field and laboratory measurements or by means of pedotransfer functions (PTFs) derived from existing soil data sets (Vereecken et al., 2010). Two points are vital in describing the SWCC and estimating the shear strength of unsaturated soil, the air entry value, ψ_{aev} and residual suction, ψ_r. Typical air-entry value for silty soil can range from 10 – 100 kPa (Lu and Griffiths, 2004).

Figure 1 below shows the variation of shear strength with matric suction. Within the linear zone, suction values are below the ψ_{aev}, the soil exhibits saturated soil behavior, and thus the ϕ^b equals ϕ'. For the non-linear zone, suction values are between the ψ_{aev} and ψ_r, ϕ^b decreases to a lower value. Here, ϕ^b may be considered as a constant value, such as $\phi^b = 0.5\ \phi'$, or may be determined from the SWCC. In the residual zone, the shear strength of unsaturated soil may remain constant, increase or decrease (Vanapalli et al., 1996; Fredlund et al., 2012). For soils that desaturate easily at low suction values such as sands and gravel, the shear strength may possibly decrease (Donald, 1956; Escario et al., 1989). Nishimura et al. (2008) established that shear strength of a silty soil was maximum at the residual suction value and reduced to less than half its maximum value within the residual zone of unsaturation.

The initial suction profile and its variation during rainfall plays a key role in evaluation of *FoS* for unsaturated slopes (Shin et al., 2013). As can be seen in Fig. 2, the suction profile varies with the prevailing surface flux boundary conditions, mainly rainfall and evaporation. For simplicity, this study considers hydrostatic conditions, thus the matric suction is mainly controlled by the hydrostatic line and the position of the groundwater table (Fredlund et al., 2012). In the past, hydrostatic conditions have been assumed to generate initial suction profiles for slopes subjected to rainfall (Tsaparas et al., 2002; Rahardjo et al., 2007; Godt et al., 2012; Oh and Lu, 2014; Qi and Vanapalli, 2015).

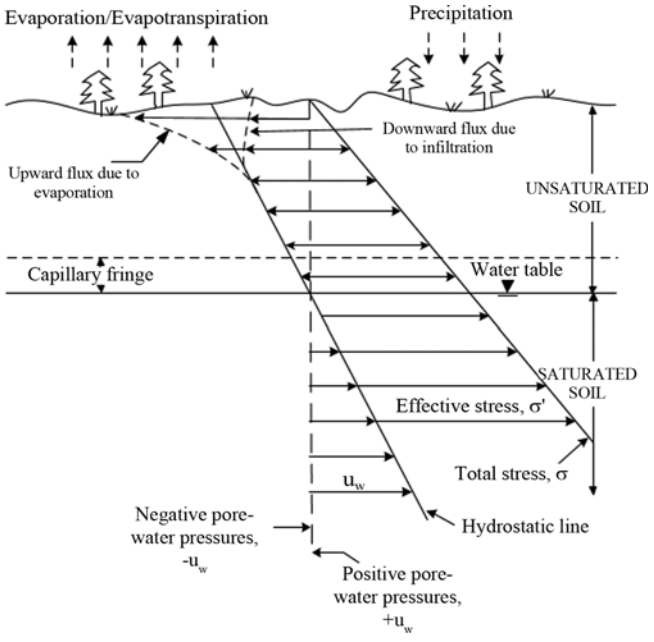

Fig. 2. Illustration of the Effect of Climatic Conditions on the Pore Water Pressure Profile Near the Ground Surface (Fredlund, 2000)

3. Numerical Modelling

With the advancement in computational methods, various numerical approaches have been developed that accurately capture advanced material behavior in the engineering field (Rabczuk and Belytschko, 2004, 2007; Rabczuk et al., 2010; Ren et al., 2016; Areias and Rabczuk, 2017; Areias et al., 2018; He et al., 2018; Zhou et al., 2018; Rabczuk et al., 2019; Cai et al., 2020). Since FEM is widely used in slope stability problems (Duncan et al., 2014), this study employed FEM software, Phase^2 (Rocscience, 2019) based on SRFEA method and Optum G2 (Optum, 2020), based on limit analysis upper and lower bound methods, for numerical simulation. The two software, based on three distinct methods, were used to benchmark against each other, thus verifying the accuracy of the results. The strength reduction method (SRM) was used to calculate the factor of safety (*FoS*) throughout this study based on two approaches described in the next section.

The boundary value problem in this study was the stability analysis of an unsaturated slope under hydrostatic conditions. The stress distribution within the soil mass followed equilibrium equations similar to Timoshenko and Goodier (1951). For compatibility, adjacent elements shared common nodes and edges with the same primary unknown distribution. The extended Mohr-Coulomb model was used to model unsaturated soil behavior. Full governing equations can be found in the Phase^2 (Rocscience, 2019) and Optum (2020) manuals.

3.1 Factor of Safety (*FoS*) Definition

Initially proposed by Bishop (1955), the strength reduction method (SRM) has been extensively used by various researchers, notably, Cheng et al. (2007), Chen et al. (2014), Tschuchnigg et al. (2015b) and Kelesoglu (2016) among others. The standard procedure assumes a Mohr Coulomb failure criterion and involves successively reducing the soil shear strength parameters using the strength reduction factor (SRF) until equilibrium can no longer be maintained. The critical SRF is the factor of safety of the slope as shown in Eq. (3) below:

$$FoS = \frac{shear\ strength}{(shear\ strength)_{mobilised}}. \tag{3}$$

The mobilized subscript signifies mobilized shear strength values on the verge of failure.

3.1.1 Strength Reduction Finite Element Analysis (SRFEA)

In SRFEA, strength reduction is executed using numerical non-convergence technique (Griffiths and Lane, 1999) and nodal displacement technique (Donald and Giam, 1988). Phase^2 and PLAXIS employ the non-convergence technique for strength reduction. Phase^2 confirms the obtained solution by carrying out a displacement check based on the nodal displacement technique (Rocscience, 2019). Phase^2 recommends that $\psi = 0$ (non-associated flow rule). For slopes with low $\phi'(< 40^o)$, the flow rule does not have a big influence on the computation of *FoS* (Tschuchnigg et al., 2015a, 2015b; Lin et al., 2020). Phase^2 has recently been used by Li and Chu (2019) and Pradhan and Siddique (2020) for stability analysis.

3.1.2 Strength Reduction Finite Element Limit Analysis (FELA)

Limit analysis approaches are based on upper and lower bound theorems of plasticity which bound the rigorous solution from above and below (Lyamin and Sloan, 2002a, 2002b). The difference between the two bounds is an exact measure of the error in the solution (Sloan, 2013). Limit analysis approaches have been widely used in geotechnical problems (Lim et al., 2017; Li et al., 2019, 2020a, 2020b). In Optum G2, associated flow rule ($\psi = \phi'$) is used. Strength reduction involves finding out the feasibility of a problem. The feasibility problem and full algorithm are discussed in detail by Krabbenhoft and Lyamin (2015). Optum G2 has recently been used in slope stability (Oberhollenzer et al., 2018) and seismic bearing capacity problems (Es-haghi et al., 2021).

3.2 2D Slope Model Development

3.2.1 Boundary Conditions

This study adopted a two-dimensional, plane-strain model for analysis. The distance between the slope and the sides of the model was at least three times the slope height, H (Gofar and Rahardjo, 2017) as illustrated in Fig. 3. Thus, the boundaries were placed far enough from the region where slope failure is likely to occur.

A free slope surface (a-f, f-e, e-d) was adopted while movement at the sides (a-b, c-d) and bottom of the slope (b-c)

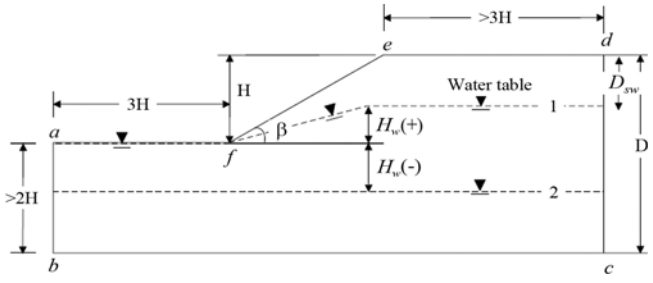

Fig. 3. Slope Boundary Conditions Used in This Study

Table 1. Mesh and Computational Details of Software in This Study

Software	No. of elements	Computation time (minutes : seconds)	Computer storage (Megabytes)
Phase^2	5,000	2:33	18
OPTUM G2	5,000	0:39[a]	3.3[a]

[a]The parameter shown is the average of lower and upper bound cases.

Table 2. Input Parameters for Verification Case 1

Category	Parameter (unit)	Value
Soil property Material model (Mohr-coulomb)	Effective cohesion, c' (kPa)	6
	Unit Weight (kN/m^3)	20
	Internal friction angle, ϕ'	45
	Dilation angle, ψ (°)	45
	Young's modulus, E (kPa)	40,000
	Poisson's ratio, v	0.3
Slope Geometry	Slope angle, β (°)	45

was restrained. In Phase^2, the auto-restrain surface option was used to assign pinned restraints to the bottom and side of the model and the surface was free. In Optum, the standard fixities option was used to define similar domain boundary conditions.

This study adopted a simplified water table shape and normalized parameter, H_w/H similar to Eid (2014) which made it convenient to indicate the water table position and quantify the corresponding effect. Also, for slope stability, the water table shape is more important within the failure surface zone compared to other areas. With reference to Fig. 3, a horizontal water was simulated by applying a constant total head on each side of the boundary as well as along a water table boundary. For an inclined water Table 1, a varying total head with height was applied along the inclining section of water table. Given that the study considered hydrostatic conditions, seepage flow and infiltration were not considered.

3.2.2 Mesh and Discretization

The discretization process in Phase^2 and Optum G2 is automated, the user only specifies the number and type of elements. Since the slope model was divided into thin layers, a fine mesh of 5,000 elements was adopted. A mesh sensitivity check for a typical slope case revealed that beyond 3,000 elements, the *FoS* and slope failure mechanism are insensitive to changes in number of elements (< 1% *FoS* difference). In Phase^2, the initial mesh settings remain fixed (no adaptivity option), by default the stability analysis was performed using a uniform mesh. The 6-noded triangular element type was chosen as recommended by the Phase^2 (Rocscience, 2019) manual.

In Optum G2, the adaptive mesh option based on advancing front type (George, 1971) was chosen which enabled the automatic allocation of more mesh elements along the failure surface region in 3 successive iterations. The mesh element type chosen was lower bound element and upper bound element described in the Optum (2020) manual.

A summary of the mesh settings and computational efficiency of the 2 software in this study is given in Table 1. The fast computation time only represents software run time and does not include slope model development and specification of mesh and input parameters which is time-consuming considering the large number of cases involved. The proposed chart solutions are comparatively quick to use and give a wider picture of the effect of unsaturated conditions. This study's computer specifications are as follows: Operating system (OS): Microsoft Windows; Edition: Windows 10 Pro; Processor: Intel(R) Core(TM) i9-7900 CPU @ 3.30 GHz, 3.31 GHz; Installed memory (RAM): 64.0 GB (63.7 GB usable); System Type : 64-bit Operating System, x64-based processor; Graphics Card: (GPU) NVIDIA GeForce RTX 2070; Hard Drive Storage Capacity: 1 TB.

3.3 Numerical Validation

3.3.1 Case 1 (No Suction)

A homogeneous 2D soil slope, from Tschuchnigg et al. (2015a) was used to validate the Phase^2 and Optum G2 numerical programs. The soil and slope input parameters are given in Table 2. Similar parameters, analysis condition (drained condition) and failure criterion (Mohr-Coulomb failure criterion) were used for verification. Unsaturated conditions were not considered.

Tschuchnigg et al. (2015a) employed PLAXIS 2D for numerical analysis and 15-node triangular element type. The *FoS* results from the Phase^2 program (1.53) and Optum G2 program (FoS_{LB} 1.517; FoS_{UB} 1.54) are almost identical to Tschuchnigg's result (*FoS* 1.53). Additionally, the failure surfaces (generated based on shear strain) in both numerical programs are relatively shallow and extend to the slope toe. This is similar to that obtained by Tschuchnigg et al. (2015a).

3.3.2 Case 2 (Experimental Test Considering Suction)

A small-scale set of landslide tests performed by Tohari et al. (2007) was used to validate the applicability of the Phase^2 and Optum G2 numerical programs to slope stability analysis incorporating unsaturated soil conditions. In total, Tohari et al. (2007) conducted 4 experiments. *FoS* results at the start of experiment 2 are used for numerical validation given the relevance to the scope of this study. The slope in experiment 2 was constructed using river sand soil. Table 3 shows the respective soil and slope parameters for the river sand. The SWCC fitting

Table 3. Soil and Slope Parameters for Verification Case 2

Category	Parameter (unit)	River sand
Soil property Mechanical Parameters	Effective cohesion, c' (kPa)	0
	Unit Weight, γ (kN/m^3)	20
	Internal friction angle, ϕ'	50
Grain size distribution parameters	Effective diameter size, d_{10} (mm)	0.175
	Coefficient of uniformity, C_u	7.14
Hydraulic parameters	Saturated hydraulic conductivity, k_{sat} (m/s)	6.4×10^{-4}
	Saturated volumetric water content, θ_s	0.48
	Residual volumetric water content, θ_r	0.048[a]
SWCC fitting parameters	α (m^{-1})	11.36
	n	3.97
Slope Geometry	Slope angle, β (°)	45
	Slope height, H (m)	0.75

[a] θ_r assumed to be 10% θ_s (Leij et al., 1996). This study adopted the extended Mohr-Coulomb model for numerical analysis.

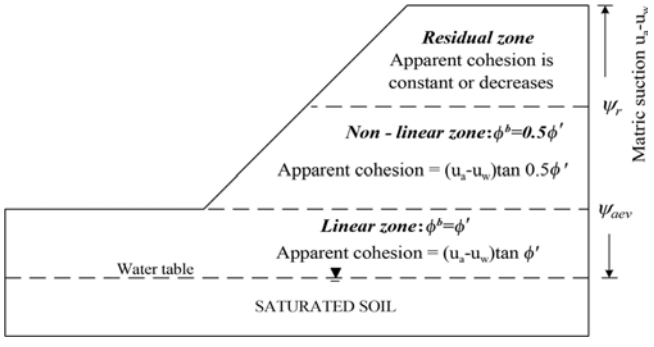

Fig. 4. Model Slope for Numerical Validation

parameters, α (m^{-1}) and n were estimated using PTFs proposed by Benson et al. (2014) based on effective diameter size, d_{60} (mm) and coefficient of uniformity, C_u.

A hydrostatic suction profile was assumed corresponding to initial slope conditions. The unsaturated portion of the slope was divided into 3 zones using the respective ψ_{aev} and ψ_r values as earlier shown in Fig. 1. Fig. 4 shows the contribution of apparent cohesion to unsaturated shear strength with varying matric suction within the slope. To account for the shear strength of unsaturated soil in the residual zone, two methods were adopted. For the 1st method, the apparent cohesion at the residual suction value was held constant while for the 2nd method, the apparent cohesion at the residual suction value was reduced by half (Donald, 1956; Nishimura et al., 2008; Fredlund et al., 2012); the 2 methods are denoted as (a) and (b) in Table 4 respectively.

In Table 4, the *FoS* results obtained from Phase^2 and Optum G2 are in agreement with the *FoS* from Tohari et al. (2007). The 2nd method (b) is seen to yield even closer results to the case study. The *FoS* % difference shown in brackets is based on comparison with the average *FoS* of the different LEM methods used by Tohari et al. (2007).

3.4 Slope Geometry and Soil Properties

Previous landslide cases involving silty soil slopes in East and South East Asia region served as a guideline for the range of parameters chosen in this study (Ng and Shi, 1998; Rahim, 2016; Tian et al., 2017; Yang et al., 2017; Nguyen et al., 2020). Table 5 gives the range of slope geometry and soil properties used in this study. The dimensionless parameter $c'/\gamma H tan\phi'$ ranging from 0 – 3 was adopted from Michalowski (2002) and encompasses a wide range of soils including silty soil. For silty soil, $c'/\gamma H tan\phi'$ ranges from 0 – 0.25. Cheng et al. (2007) showed that *FoS* is fairly insensitive to changes in soil elastic parameters, i.e., Young's modulus, E, and Poisson's ratio, ν. Only one set of elastic parameters was used.

3.5 Quantifying Effect of Matric Suction Using Total Cohesion Method

This study is based on hydrostatic pore pressure condition.

Table 4. Summary of *FoS* Comparison Results

Method	Factor of Safety, *FoS* (at the start of experiment 2)					
	Tohari et al. (2007)				Phase^2	Optum G2[a]
	Ordinary	Bishop	Janbu	Spencer		
a	1.280	1.353	1.279	1.348	1.400 (6.0%)	1.400 (6.0%)
b					1.360 (3.4%)	1.355 (3.0%)

[a] *FoS* is the average of upper bound and lower bound results

Table 5. Parameters Chosen for This Study

Category	Parameter (unit)	Range of Values	References
Soil property	$c'/\gamma H tan\phi'$ (dimensionless)	0.0 – 3.0	(Michalowski, 2002) (Yang et al., 2021)
Material model (Extended Mohr-Coulomb)	Matric suction angle, ϕ^b (°)	$\phi^b = \phi'$ $(u_a - u_w) < \psi_{av}$ $\phi^b = 0.5\phi'$ $(u_a - u_w) > \psi_{aev}$	(Leong et al., 2003)
	Air-entry value, ψ_{aev} (kPa)	30 – 100	(Lu and Griffiths, 2004)
	Dilation angle, ψ (°)	Non-associated Flow Rule ($\psi = 0$)	(Rocscience, 2019)
		Associated Flow Rule ($\psi = \phi'$)	(Optum, 2020)
	Young's modulus, E (kPa)	20,000	(Bowles, 1997)
	Poisson's ratio, ν	0.3	
Slope Geometry	H_w/H	(-2.0) – (0.7)	(Yang et al., 2021)
	Slope angle, β (°)	15 - 40	

Therefore, the authors assumed a linear relationship between pore pressures and the distance from the water table. Consequently, matric suction (equivalent to negative pore water pressure, $-u_w$) was mainly dependent on the hydrostatic profile and position of the water table. See Fig. 5.

For a typical slope, the soil stratigraphy was subdivided into layers. The cohesion due to matric suction was obtained by multiplying the average matric suction for a soil layer by $\tan\phi^b$. This apparent cohesion value was added to the effective cohesion, c', and the total cohesion, c, assigned to respective soil layers in each numerical program (Phase^2 and Optum G2) for slope stability analysis.

This total cohesion method by Ching et al. (1984) enables input of values based on the user's choice thereby bypassing any uncertainties or inherent limitations in the numerical programs in accommodating unsaturated soil behavior. On the flip side, the only drawback of this method is having to manually compute and input the total cohesion, c, for each layer (Fredlund et al., 2012).

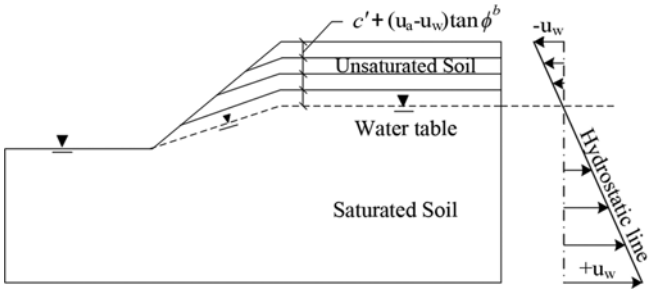

Fig. 5. Typical Slope Model with Subdivided Soil Stratigraphy

4. Results and Discussion

The contribution of unsaturated soil conditions to the stability of the slope is examined in this study. Generally speaking, results from Phase^2 and Optum G2 numerical programs are in good agreement even though Optum G2 yields slightly higher *Fos* results compared to Phase^2, particularly for steeper slope angles ($\beta \geq 30°$), which could be attributed to the flow rule (Tschuchnigg et al., 2015b). The results from Optum G2 are the average of FoS_{LB} and FoS_{UB}. On average, the difference between FoS_{LB} and FoS_{UB} is about 1%. The slope failure surfaces based on shear strain for different conditions are also discussed.

4.1 Effect of Soil and Slope Parameters on *FoS*

4.1.1 Effect of Soil Properties on *FoS*

Focus is placed on the air-entry value, ψ_{aev} since the effects of mechanical parameters c', ϕ' and γ on slope stability are already well documented in past literature. Generally, the air-entry value, ψ_{aev} gives an indication of the fines content in a soil sample. A high ψ_{aev} translates to higher fines content and greater contribution of cohesion, c, to slope stability. A comparison of ψ_{aev} with *FoS* for different water table positions shown in Fig. 6(a), reveals that the effect of ψ_{aev} on *FoS* is contingent upon the location of the water table, H_w/H. It is observed that for slopes with a high water table location, the influence of ψ_{aev} on *FoS* is minimal. However, the effect of ψ_{aev} on *FoS* increases for slopes with a lower water table. This finding is limited to the range of ψ_{aev} studied, therefore more investigation would be required in the future.

4.1.2 Effect of Water Table Location H_w/H

The effect of groundwater table location on slope stability for different suction conditions is illustrated in Fig. 6(b). For no suction condition, the *FoS* is only sensitive to changes in water table depth for cases with high groundwater position, $H_w/H \geq$

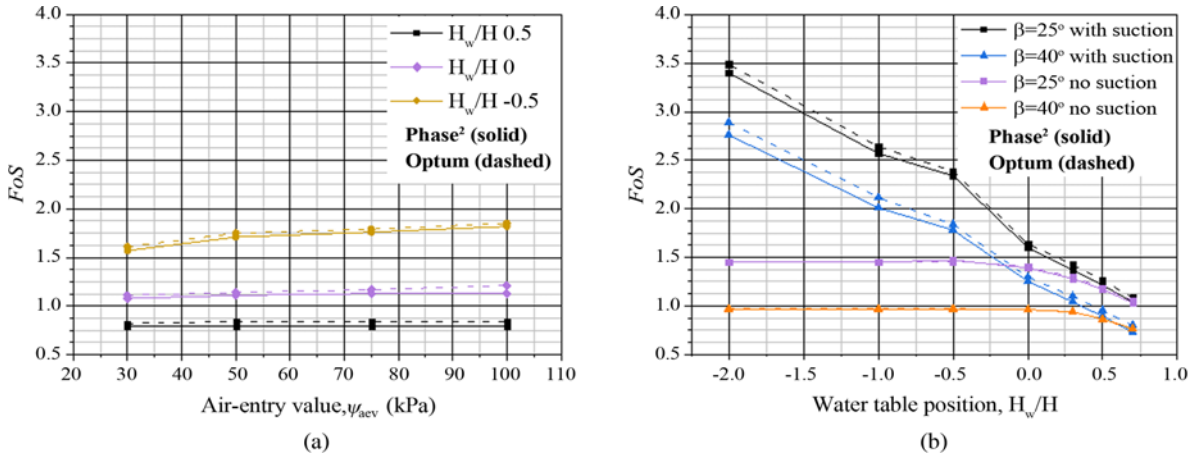

Fig. 6. Effect of Soil Properties on *FoS*: (a) Relationship between ψ_{aev} and *FoS* for Slope with $\beta = 25^{\circ}$, $c'/\gamma H tan\phi = 0.02$, (b) Relationship between Groundwater Table, H_w/H and *FoS* for Slope with $\beta = 25^{\circ}$, 40°, $c'/\gamma H tan\phi = 0.08$, $\psi_{aev} = 50$ kPa

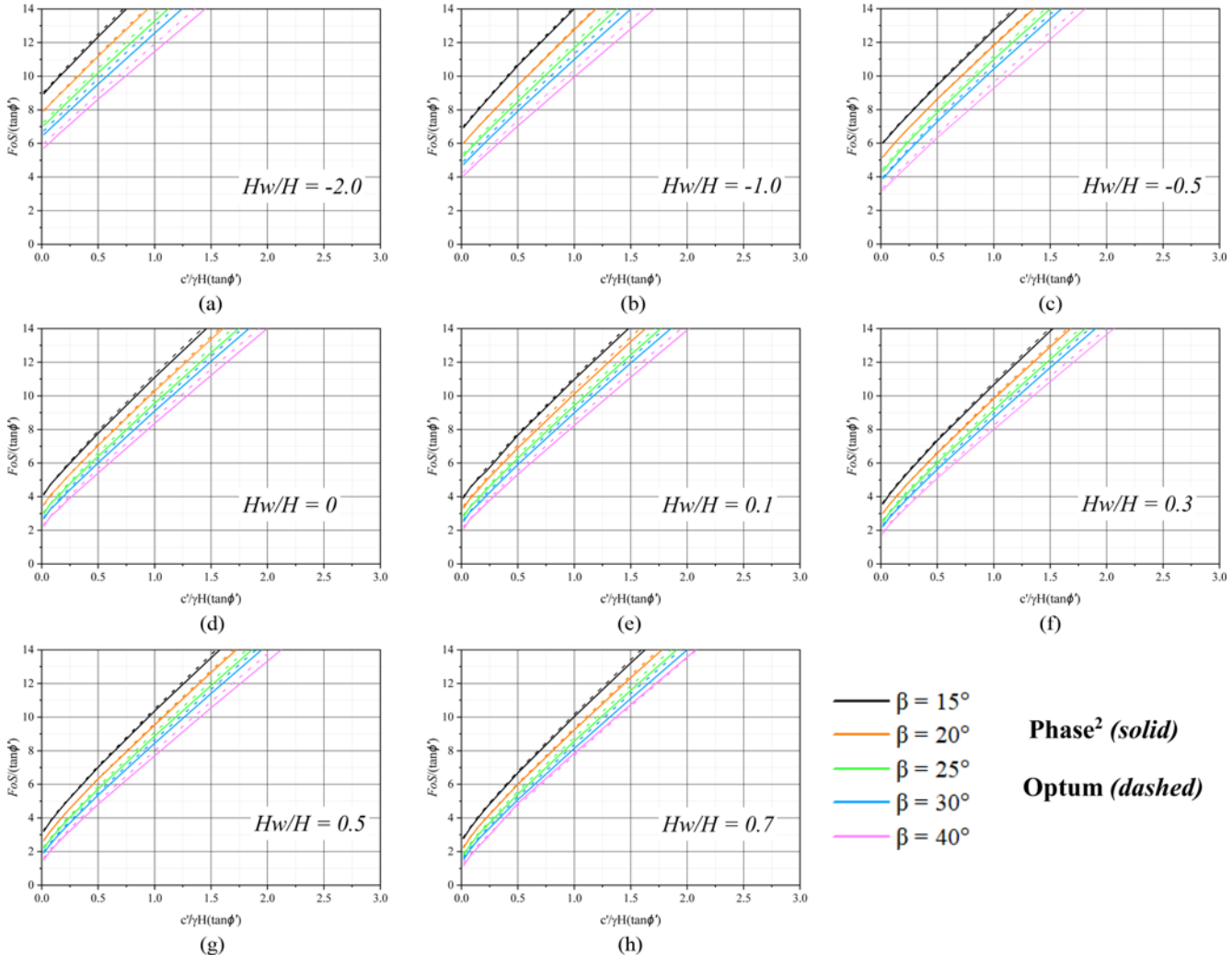

Fig. 7. Stability Charts for Unsaturated Soil, $\psi_{aev} = 30$ kPa: (a) $H_w/H = -2.0$, (b) $H_w/H = -1.0$, (c) $H_w/H = -0.5$, (d) $H_w/H = 0$, (e) $H_w/H = 0.1$, (f) $H_w/H = 0.3$, (g) $H_w/H = 0.5$, (h) $H_w/H = 0.7$

0.25. For $H_w/H \leq 0.0$, the *FoS* does not change with water table depth, since the propagation of the failure surface is no longer affected by the water table and the total cohesion, c, in the unsaturated zone remains constant (equal to effective cohesion, c'). Contrarily, with incorporation of suction conditions, the *FoS* continually increases with the depth of the water table due to the increasing contribution of apparent cohesion to unsaturated soil strength.

For this study, it is established that for slopes with water table depth less than 5 m from the ground surface, the effect of apparent cohesion may be ignored. Within such slopes, a major portion of the failure surface is below the water table thus contribution of suction to unsaturated soil strength is negligible. This is seen in Fig. 6(b), for $H_w/H > 0.5$, where cases with suction and no suction conditions have similar *FoS*, with less than 1% difference. Of more practical importance is the contribution of apparent cohesion in slopes that are neither too safe to fail nor already at collapse. Fig. 6(b) reveals that such slope cases fall within the range, $\beta = 25 - 40^{o}$ and water table location, $H_w/H = 0.5 - (-0.5)$. This can be confirmed by the chart solutions shown in Figs. 7 – 10 for $c'/\gamma H tan\phi' = 0 - 0.25$, corresponding to approximate silty soil range. The chart solutions presented in this study, follow the format by Michalowski (2002). As seen in Figs. 7 – 10, four sets of charts solutions are proposed for each ψ_{aev}, 30, 50, 75, 100 kPa and are validated using a case from a previous study.

4.1.3 Effect of Slope Geometry

The effect of slope angle, β on *FoS* for different internal friction angle, ϕ' and suction conditions is shown in Fig. 11(a). The difference in *FoS* between cases with suction and no suction is constant with increase in slope angle, β. For example, for $\phi' = 25^{o}$, the *FoS* percentage difference between suction and no suction cases is about 6% in Optum G2 and 3% in Phase^2. For $\phi' = 35^{\circ}$, the *FoS* percentage difference between suction and no suction cases is about 7% in Optum G2 and 4% in Phase^2. The contribution of suction to *FoS* is pertinent to all slope angles considered in this study.

The relationship between the slope height, H and *FoS* is shown in Fig. 11(b). With increase in slope height, H, the *FoS*

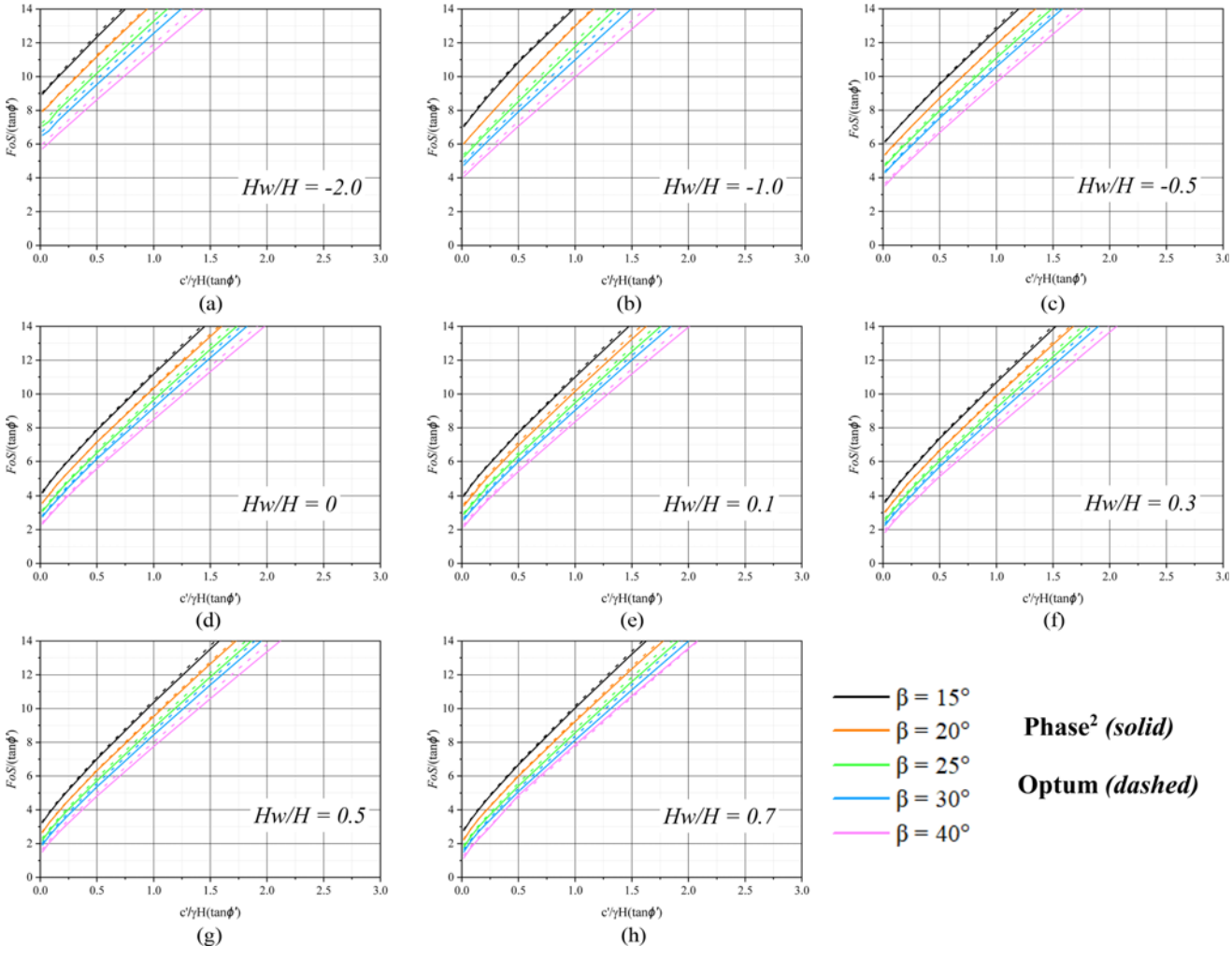

Fig. 8. Stability Charts for Unsaturated Soil, $\psi_{aev} = 50$ kPa: (a) $H_w/H = -2.0$, (b) $H_w/H = -1.0$, (c) $H_w/H = -0.5$, (d) $H_w/H = 0$, (e) $H_w/H = 0.1$, (f) $H_w/H = 0.3$, (g) $H_w/H = 0.5$, (h) $H_w/H = 0.7$

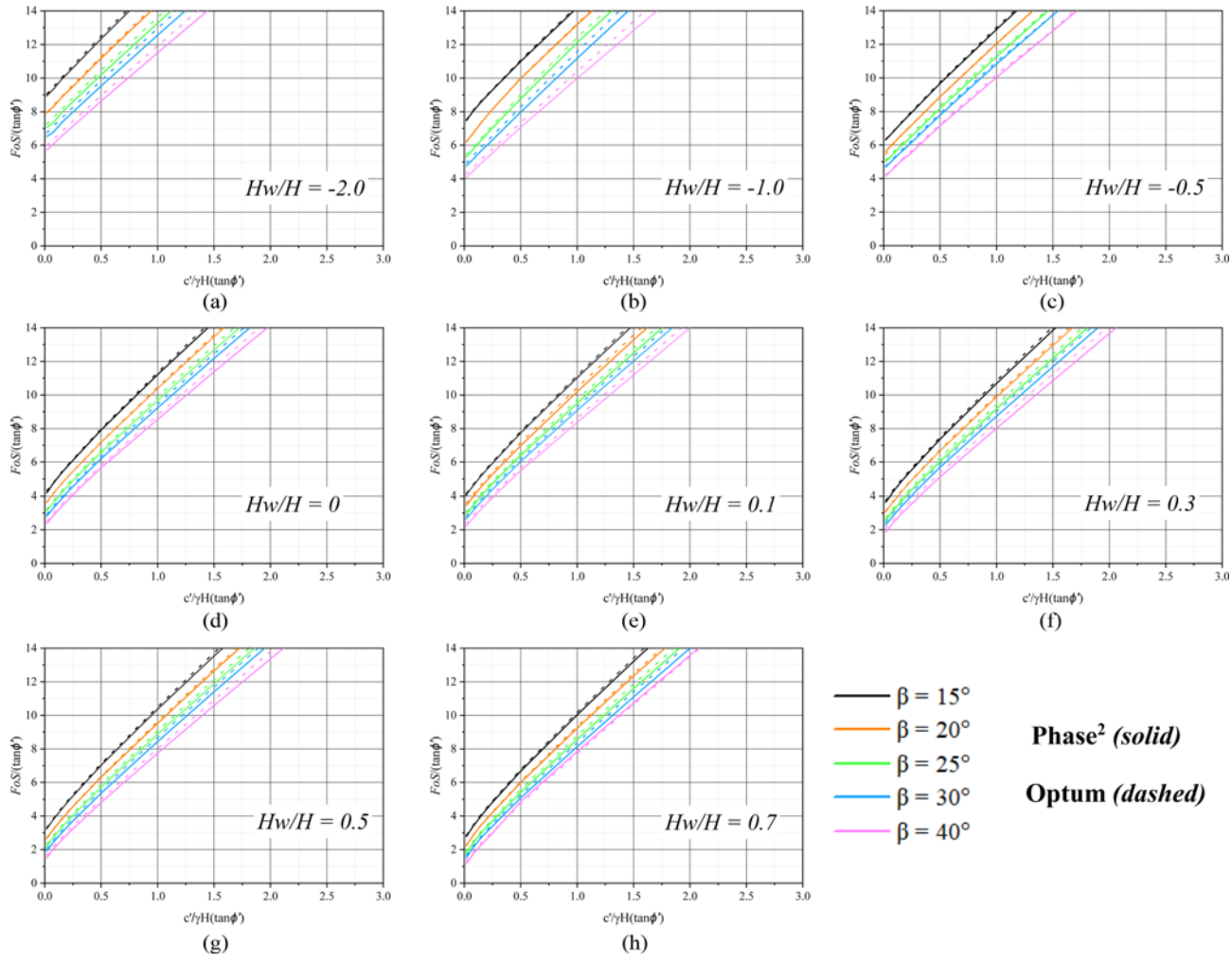

Fig. 9. Stability Charts for Unsaturated Soil, ψ_{aev} = 75 kPa: (a) H_w/H= -2.0, (b) H_w/H = -1.0, (c) H_w/H = -0.5, (d) H_w/H = 0, (e) H_w/H = 0.1, (f) H_w/H = 0.3, (g) H_w/H = 0.5, (h) H_w/H = 0.7

decreases exponentially. At the same time, the effect of suction and by extension apparent cohesion on the *FoS* diminishes, since the no suction and with suction conditions yield relatively similar *FoS* at larger slope heights, H > 30 m. At such slope heights, the effect of apparent cohesion may be ignored.

The comparison of different parameters with suction and no suction condition reveals that the contribution of apparent cohesion to *FoS* is most noticeable with changes in water table location.

4.2 Applicability of Stability Charts

A parametric study by Rahardjo et al. (2007) highlighting the importance of different parameters (Toll et al., 1999) in assessing slope instability under different rainfall condition is used for validation of the charts solutions proposed in this study. The soil shear strength properties used included, c' = 10 kPa, ϕ' = 26°, ϕ^b = 26°, and unit weight, γ = 20 kN/m^3, based on typical values encountered in a few Singapore sites.

For initial conditions, hydrostatic condition was assumed with a negative pore pressure cut-off of -75 kPa based on measured suction values in Singapore. To simulate rainfall infiltration, seepage analysis was performed using SEEP/W by Geo-Slope (1998a) and the pore pressures obtained exported to SLOPE/W by Geo-Slope (1998b) for slope stability analysis via Bishop's simplified method. The results were given in terms of factor of safety for initial conditions, $FoS_{(ini)}$, and *FoS* for different rainfall intensities. The slope model adopted by Rahardjo et al. (2007) is shown in Fig. 12. The case used to validate the chart solutions involved silty soil properties (study series A) and was based on initial conditions prior to rainfall since this study assumes hydrostatic conditions.

4.2.1 Case Study

Consider a slope with slope geometry parameters, H = 10 m, β = 26.6° and 33.7°, and silty soil properties, c' = 10 kPa, ϕ' = 26°, ϕ^b = 26°, ψ_{aev} = 50 kPa, H_w = -5 m; H_w/H = -0.5. Fig. 13 gives the procedure of using the stability charts.

Figure 14 shows the estimated $FoS/tan\phi'$ values for β, 26.6° and 33.7°. Table 6 below is a summary of the *FoS* for the chart solutions and the comparison to the *FoS* of the reference paper.

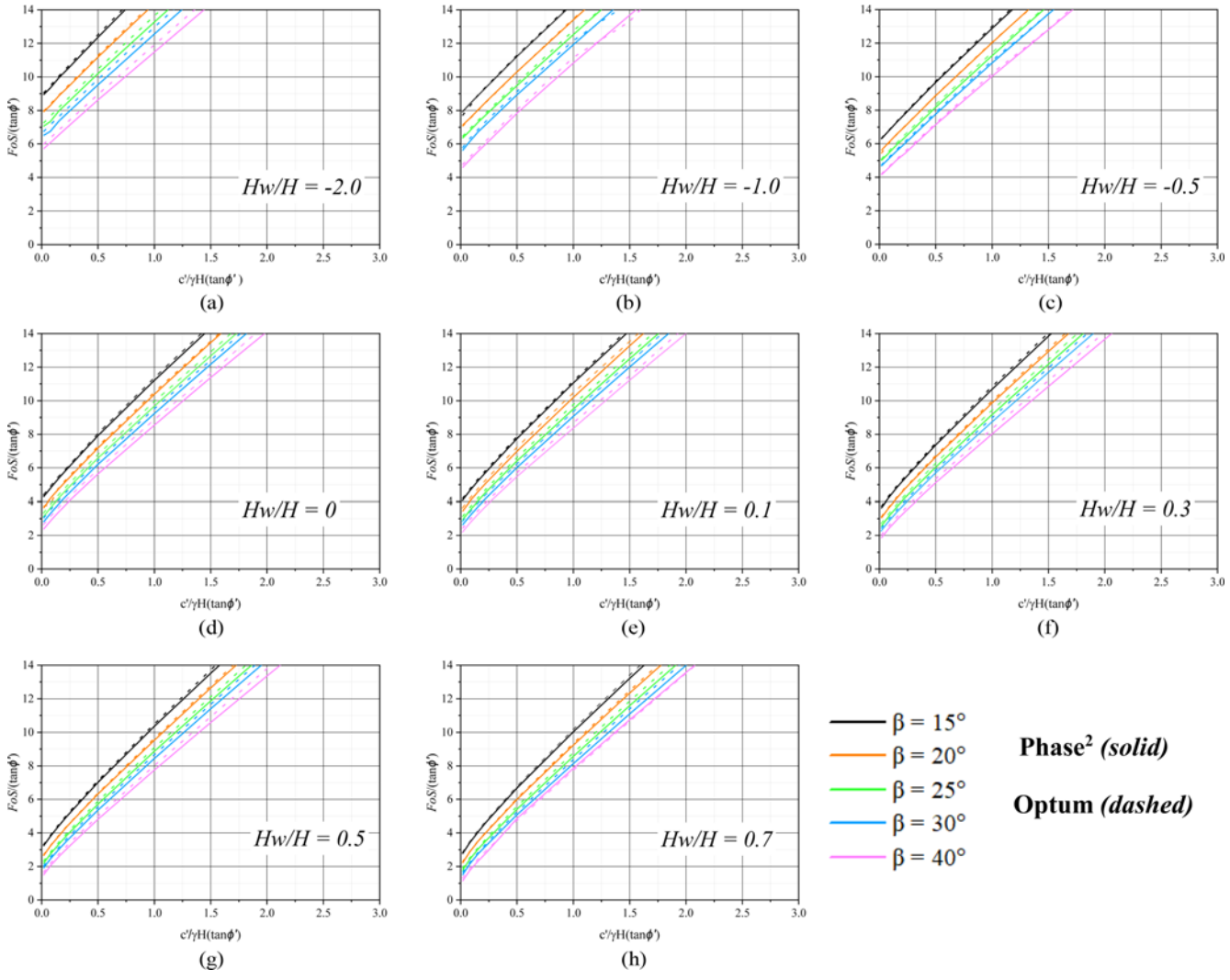

Fig. 10. Stability Charts for Unsaturated Soil, ψ_{aev} = 100 kPa: (a) H_w/H = -2.0, (b) H_w/H = -1.0, (c) H_w/H = -0.5, (d) H_w/H = 0, (e) H_w/H = 0.1, (f) H_w/H = 0.3, (g) H_w/H = 0.5, (h) H_w/H = 0.7

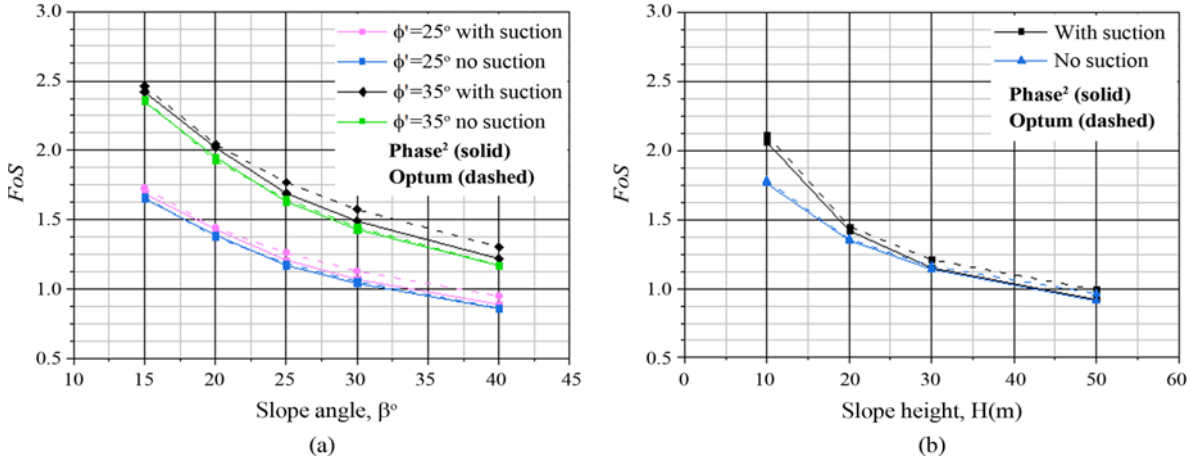

Fig. 11. Effect of Slope Geometry on *FoS*: (a) Relationship between Slope Angle, β and *FoS* for Slope with $c'/\gamma H$ = 0.03, H_w/H = 0.5, ψ_{aev} = 50 kPa, (b) Relationship between Slope Height and *FoS* for slope with β = 25°, $c'/\gamma H tan\phi'$ = 0.06, Water Table Depth, 10 m, ψ_{aev} = 50 kPa

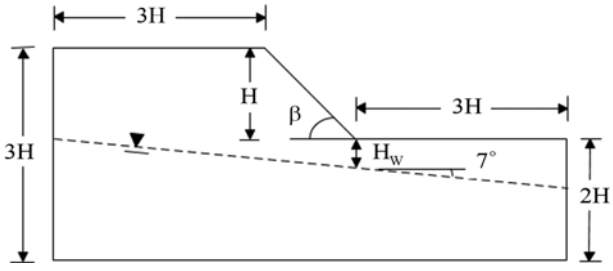

Fig. 12. Slope Model Used by Rahardjo et al. (2007)

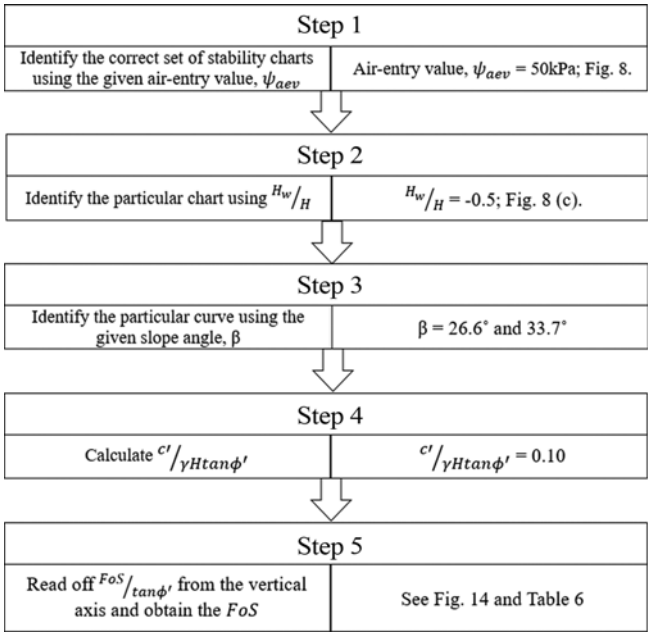

Fig. 13. Flowchart Showing Procedure of Using Stability Charts

The *FoS* percentage difference in reference to Rahardjo et al. (2007) is shown in brackets. Results from PLAXIS 2D which uses the SRFEA technique are also included for comparison purposes. In Table 6, the chart solutions are able to estimate *FoS* values with reasonable accuracy.

It should be noted that matric suction angle, ϕ^b adopted in this study and by Rahardjo et al. (2007) are distinct although *FoS* from various methods in Table 6 are similar. For a typical silty slope H = 10 m, β = 30°, H_w/H = -0.5, c' = 5 kPa, ϕ' = 32°, ψ_{aev} = 75 kPa under hydrostatic conditions, there are 2 different scenarios. In the first scenario, the relation $\phi^b = 0.5\phi'$ when $(u_a - u_w) > \psi_{aev}$ is used, as adopted in this study. The second scenario, the relation $\phi^b = \phi'$ for all suction values with a negative pore pressure cutoff of -75 kPa is used, as adopted by Rahardjo et al. (2007).

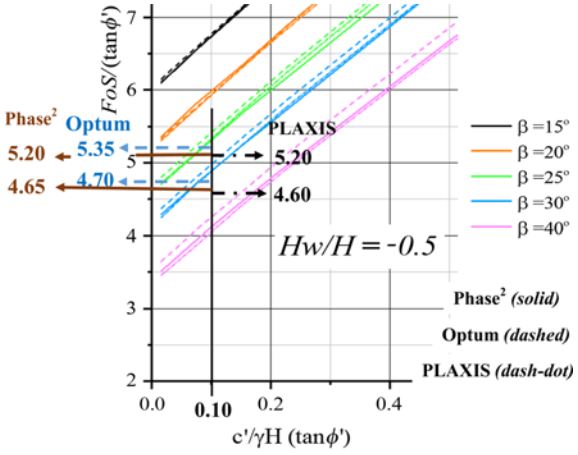

Fig. 14. Magnified Stability Chart for ψ_{aev} = 50 kPa, H_w/H = -0.5

Scenario (1): $\phi^b = 0.5\phi'$ when $(u_a - u_w) > \psi_{aev}$. At 7.5 m above the water table, $(u_a - u_w)$ = 73.58 kPa, the apparent cohesion, 73.58 (tan32°) = 45.97 kPa. At 15 m above the water table, $(u_a - u_w)$ = 147.15 kPa, ($>\psi_{aev}$ = 75 kPa), the apparent cohesion, 147.15 (tan16°) = 42.19 kPa.

Scenario (2): $\phi^b = \phi'$ for all suction values with a suction cut-off of 75 kPa. At 7.5m above the water table, $(u_a - u_w)$ = 73.58 kPa, the apparent cohesion, 73.58 (tan32°) = 45.97 kPa, same as scenario 1. At 15 m above the water table, $(u_a - u_w)$ = 75 kPa due to the imposed suction cut-off; thus, apparent cohesion, 75 (tan32°) = 46.86 kPa.

The conservative relation $\phi^b = 0.5\phi'$ when $(u_a - u_w) > \psi_{aev}$ adopted in this study is seen to be effective in reducing apparent cohesion. For $(u_a - u_w) > \psi_{aev}$, the apparent cohesion $(u_a - u_w)tan\phi^b$ is significantly reduced, almost by half. This counterbalances the effect of a negative pore pressure cutoff of -75 kPa as used by Rahardjo et al. (2007). Evidently, scenario (1) can be considered slightly more conservative than scenario (2) explaining why the chart results are slightly more conservative than Rahardjo et al. (2007) results. It is suggested that the proposed charts are limited to slopes with water table location up to 30m from the ground surface.

Other reasons for the slight differences in *FoS* could be due to the difference in orientation of the water-table. Rahardjo et al. (2007) adopted a water table inclining at 7° as seen in Fig. 12. This study adopted a straight horizontal water table orientation as shown in Fig. 3. Also, Rahardjo et al. (2007) slope stability analysis used Bishop's simplified method (based on LEM). Phase^2 and PLAXIS use the SRFEA technique and Optum G2 uses FELA. Generally, Optum G2 yielded slightly higher *FoS*

Table 6. Summary of *FoS* Comparison from Rahardjo Case

Slope Angle, β	Factor of Safety (*FoS*)			
	(Rahardjo et al., 2007)	Phase^2	Optum G2	PLAXIS 2D
26.6°	2.55	2.54 (-0.4%)	2.61 (2.3%)	2.54 (-0.4%)
33.7°	2.38	2.27 (-4.7%)	2.29 (-3.7%)	2.24 (-5.7%)

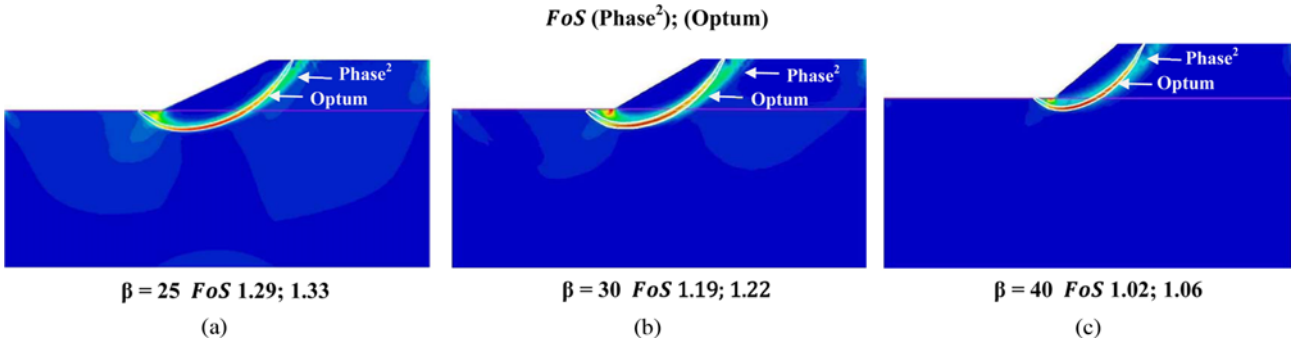

Fig. 15. Slope Failure Surface for Different β^{o} (H_w/H = 0, ψ_{aev} = 50 kPa, c′/γH(tanϕ) = 0.08): (a) β = 25, (b) β = 30, (c) β = 40

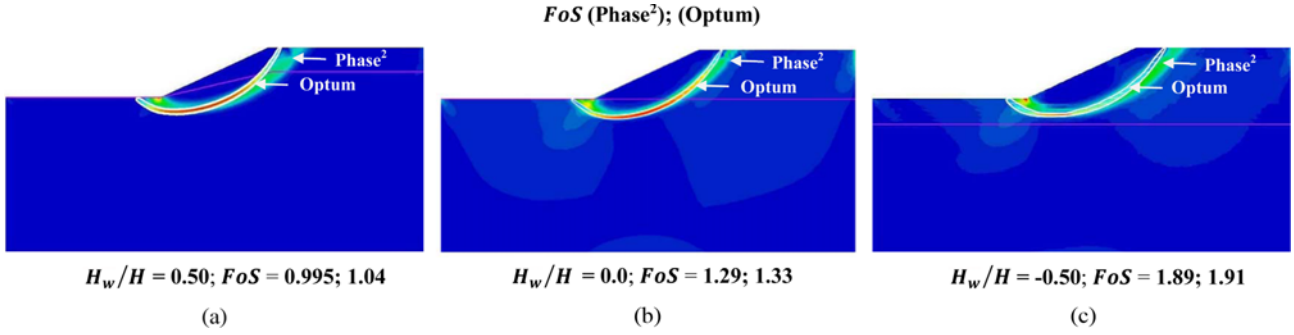

Fig. 16. Slope Failure Surfaces for Different H_w/H (β = 25°, ψ_{aev} = 50 kPa, c′/γH (tanϕ) = 0.08): (a) H_w/H = 0.5, (b) H_w/H = 0.0, (c) H_w/H = -0.5

for relatively steeper slopes, $\beta \geq 30^{o}$, compared to Phase^2 and PLAXIS, whose results are almost identical and are the most conservative.

4.3 Development of Failure Surfaces

The failure mechanisms examined for both Phase^2 and Optum G2 were limited to slopes cases of practical engineering importance, particularly, $\beta = 25 - 40^{o}$ and $H_w/H = 0.5 - (-0.5)$ within silty soil range $(c')/\gamma H tan\phi' = 0 - 0.25$, considering suction condition. Within this range, the toe failure mechanism is most dominant which is characteristic of cohesive-frictional soil slopes (Gao et al., 2013; Duncan et al., 2014). The failure surfaces in Optum G2 are much finer due to mesh adaptivity. For clarity, the failure surfaces from both software are shown in one figure. The pink line represents the water table. The following findings were made from the results:

1. As can be seen in Fig. 15, the depth of the failure surface decreases with an increase in slope angle, β^{o}. This trend was more pronounced compared to other parameters.
2. As H_w/H ratio reduces, implying increasing unsaturated layer depth, the failure surface depth increased, as shown in Fig. 16. The increase in depth of the failure surface is attributable to the presence of negative pore water pressures in the unsaturated soil layer which translates to greater cohesion, c.
3. An increase in ψ_{aev} increased the depth of the failure surface for slopes with a deep water table due to larger matric suction which translates to greater cohesion, c. For slopes with a shallow water table, and negligible negative pore pressures, the size of the failure surface remained the same with change in ψ_{aev}. As a general rule, increase in cohesion leads to increase in depth of the failure surface, while an increase in ϕ', yields shallower failure surfaces, as shown by Jiang and Yamagami (2008), Duncan et al. (2014) and Lin and Chen (2017) relating the dimensionless shear strength parameter, $\lambda_{c\phi} = c'/\gamma H tan\phi'$ to the depth of the failure surface.

4.4 Sensitivity Assessment

A sensitivity assessment was conducted to quantify the influence

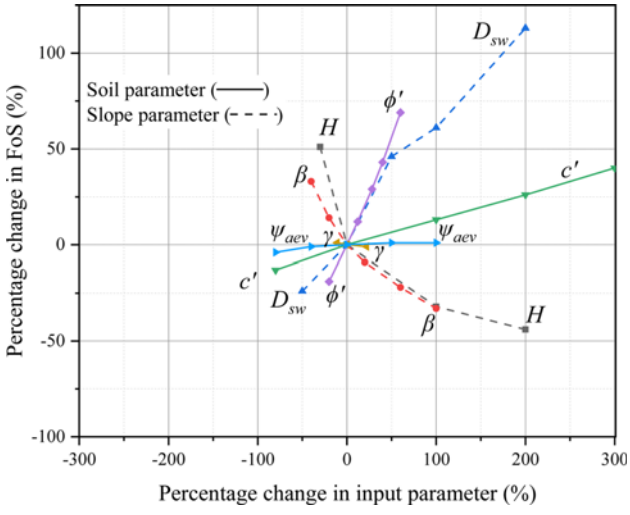

Fig. 17. Sensitivity Assessment of Input Parameters

of input parameters on the *FoS*, the output parameter of interest. The parameters were expressed in terms of percentage change (%) with reference to a baseline case. In Fig. 17, it is seen that H, β, ϕ' and D_{sw} have the most significant influence on the *FoS*. The latter, D_{sw}, (in normalized form H_w/H) has a direct effect on the contribution of apparent cohesion to slope stability. γ and ψ_{aev} have the least influence on the *FoS*. It should be noted that these trends are limited to the range of parameters used in this study.

5. Conclusions

This study adopted the total cohesion method to investigate the contribution of apparent cohesion to the stability of silty slopes under hydrostatic conditions. The following conclusions can be made based on the results of this study:

1. Results from the numerical validation cases demonstrate that Phase^2 and Optum G2 can accurately carry out stability analysis for both conventional and unsaturated conditions. *FoS* results from Phase^2 and Optum G2 are in good agreement; however, Optum G2 yields slightly higher *FoS* compared to Phase^2 particularly for relatively steep slopes, $\beta \geq 30^o$.
2. Under hydrostatic conditions, the contribution of apparent cohesion to *FoS* of a slope is most conspicuous while varying the water table position, H_w/H. The contribution of apparent cohesion to *FoS* may be ignored for slopes with a water table depth less than 5 m or slope height, $H \geq 30$ m.
3. For convenience, the results are presented in the form of stability charts which are validated using a case from a previous study. The proposed set of charts give reasonably close *FoS* results to the case study, thus, they can be used for quick assessment of *FoS* for unsaturated silty slopes. The limitation is that the effect of rainfall infiltration and seepage is not incorporated in the chart solutions.
4. The dominant failure mechanism is the toe failure mechanism. An investigation into the effect of different slope and soil parameters on the depth of the failure surface reveals that the slope angle, β^o, water table depth, H_w/H and by extension, cohesion, c, have the most influence on the depth of the failure surface. The influence of ψ_{aev} on depth of failure surface is dependent on H_w/H.

Acknowledgments

The 2nd author is grateful for the financial support provided for his PhD study through the National Taiwan University of Science and Technology (NTUST) scholarship.

Nomenclature

c = Total cohesion (kPa)
c' = Effective cohesion (kPa)
C_u = Coefficient of uniformity d_{60}/d_{10}
D_{sw} = Water table depth
d_{10}, d_{60} = Effective grain size 10%, 60% passing
E = Soil Young's modulus (kPa)
FELA = Finite element limit analysis
FEM = Finite element method
FoS = Factor of safety
$FoS_{(ini)}$ = Initial factor of safety
$FoS_{LB,\ UB}$ = Factor of safety lower bound, upper bound
H = Slope height (m)
H_w = Vertical distance of water table to slope toe (m)
k_s = Saturated hydraulic conductivity (m/s)
LEM = Limit equilibrium method
n = SWCC fitting parameter related to pore size distribution (dimensionless)
SRF = Strength reduction factor
SRFEA = Strength reduction finite element analysis
SRM = Strength reduction method
SWCC = Soil water characteristic curve
u_a = Pore air pressure (kPa)
u_w = Pore water pressure (kPa)
α = SWCC fitting parameter related to air entry value (kPa^{-1})
β = Slope inclination (^{o})
γ = Unit weight of the soil (kN/m^3)
θ_r = Residual volumetric water content
θ_s = Saturated volumetric water content
$\lambda_{c\phi}$ = Shear strength parameter (dimensionless)
ν = Poisson's ratio
ϕ' = Internal friction angle (°)
ϕ^b = Matric suction angle (^{o})
ψ = Soil dilation angle (^{o})
ψ_{aev} = Air-entry value (kPa)
ψ_r = Residual suction (kPa)

ORCID

Joram Wachira Mburu https://orcid.org/0000-0002-3447-9676

References

Areias P, Rabczuk T (2017) Steiner-point free edge cutting of tetrahedral meshes with applications in fracture. *Finite Elements in Analysis and Design* 132:27-41, DOI: 10.1016/j.finel.2017.05.001

Areias P, Reinoso J, Camanho PP, César de Sá J, Rabczuk T (2018) Effective 2D and 3D crack propagation with local mesh refinement and the screened Poisson equation. *Engineering Fracture Mechanics* 189:339-360, DOI: 10.1016/j.engfracmech.2017.11.017

Benson CH, Chiang I, Chalermyanont T, Sawangsuriya A (2014) Estimating van Genuchten parameters α and n for clean sands from particle size distribution data. Geo-Congress 2014, February 23-26, Atlanta, GA, USA

Bishop AW (1955) The use of the Slip Circle in the stability analysis of slopes. *Géotechnique* 5:7-17, DOI: 10.1680/geot.1955.5.1.7

Bowles JE (1997) Foundation analysis & design. McGraw-Hill, Singapore

Brand EW (1984) Landslides in Southeast Asia: A state-of-art report. Proceedings of the 4th international symposium on landslides, September 16-21, Toronto, Canada, 377-384

Cai G, Li M, Han B, Di K, Liu Q, Li J (2020) Numerical analysis of unsaturated soil slopes under rainfall infiltration based on the modified glasgow coupled model. *Advances in Civil Engineering* 2020:8865179, DOI: 10.1155/2020/8865179

Chae J, Kim B, Park SW, Kato S (2010) Effect of suction on unconfined compressive strength in partly saturated soils. *KSCE Journal of Civil Engineering* 14(5):281-290, DOI: 10.1007/s12205-010-0281-7

Chen J, Liu J, Xue J, Shi Z (2014) Failure analyses of a reinforced embankment by strength reduction and limit equilibrium methods considering hardening of soft clay. *KSCE Journal of Civil Engineering* 18(11):2043-2050, DOI: 10.1007/s12205-014-0288-6

Cheng YM, Lansivaara T, Wei WB (2007) Two-dimensional slope stability analysis by limit equilibrium and strength reduction methods. *Computers and Geotechnics* 34:137-150, DOI: 10.1016/j.compgeo.2006.10.011

Ching RKH, Sweeney DJ, Fredlund D (1984) Increase in factor of safety due to soil suction for two Hong Kong slopes. Proceedings of the fourth international symposium on landslides, September 16-21, Toronto, Canada

Donald IB (1956) Shear strength measurements in unsaturated non-cohesive soils with controlled negative pore pressures. Proceedings of 2nd Australia-New Zealand conference on soil mechanics and foundation engineering, Christchurch, New Zealand

Donald IB, Giam SK (1988) Appliaction of the nodal displacement method to slope stability analysis. 5th Australia-New Zealand conference on geomechanics, Sydney, Australia, 456-460

Duncan JM, Wright SG, Brandon TL (2014) Soil strength and slope stability. Wiley, Hoboken, NJ, USA

Eid HT (2014) Stability charts for uniform slopes in soils with nonlinear failure envelopes. *Engineering Geology* 168:38-45, DOI: 10.1016/j.enggeo.2013.10.021

Es-haghi MS, Abbaspour M, Rabczuk T (2021) Factors and failure patterns analysis for undrained seismic bearing capacity of strip footing above void. *Internation Journal of Geomechanics* 21:04021188, DOI: 10.1061/(ASCE)GM.1943-5622.0002166

Escario V, Juca JFT, Coppe MS (1989) Strength and deformation of partly saturated soils. *Congrès International de Mécanique Des Sols et Des Travaux de Fondations* 12:43-46

Finch HJS, Samuel AM, Lane GPF (2014) 3 - Soils and soil management . In: Lockhart & Wiseman's crop husbandry including grassland (ninth edition). Woodhead Publishing, Cambridge, UK

Fourie AB (1996) Predicting rainfall-induced slope instability. *Proceedings of the Institution of Civil Engineers - Geotechnical Engineering* 119(4):211-218, DOI: 10.1680/igeng.1996.28757

Fredlund DG (2000) The 1999 R.M. Hardy Lecture: The implementation of unsaturated soil mechanics into geotechnical engineering. *Canadian Geotechnical Journal* 37:963-986, DOI: 10.1139/t00-026

Fredlund DG, Morgenstern NR, Widger RA (1978) The shear strength of unsaturated soils. *Canadian Geotechnical Journal* 15:313-321, DOI: 10.1139/t78-029

Fredlund DG, Rahardjo H, Fredlund MD (2012) Unsaturated soil mechanics in engineering practice. Wiley, Hoboken, NJ, USA

Gao Y, Zhang F, Lei GH, Li D, Wu Y, Zhang N (2013) Stability charts for 3D failures of homogeneous slopes. *Journal of Geotechnical and Geoenvironmental Engineering* 139:1528-1538, DOI: 10.1061/(ASCE)GT.1943-5606.0000866

Geo-Slope (1998a) SEEP/W for finite element seepage, user's guide. International Geo-Slope, Calgary, Canada

Geo-Slope (1998b) SLOPE/W for stability analysis, user's guide. International Geo-Slope, Calgary, Canada

George JA (1971) Computer implementation of the finite element method. PhD Thesis, Stanford University, Stanford, CA, USA

Godt JW, Şener-Kaya B, Lu N, Baum RL (2012) Stability of infinite slopes under transient partially saturated seepage conditions. *Water Resources Research* 48(5), DOI: 10.1029/2011WR011408

Gofar N, Rahardjo H (2017) Saturated and unsaturated stability analysis of slope subjected to rainfall infiltration. *MATEC Web of Conferences* 101:05004, DOI: 10.1051/matecconf/201710105004

Griffiths DV, Lane PA (1999) Slope stability analysis by finite elements. *Géotechnique* 49:387-403, DOI: 10.1680/geot.1999.49.3.387

Han Zh, Vanapalli SK (2016) State-of-the-art: Prediction of resilient modulus of unsaturated subgrade soils. *Internation Journal of Geomechanics* 16:04015104, DOI: 10.1061/(ASCE)GM.1943-5622.0000631

He P, Li SC, Xiao J, Zhang QQ, Xu F, Zhang J (2018) Shallow sliding failure prediction model of expansive soil slope based on gaussian process theory and its engineering application. *KSCE Journal of Civil Engineering* 22(5):1709-1719, DOI: 10.1007/s12205-017-1934-6

Jiang JC, Yamagami T (2008) A new back analysis of strength parameters from single slips. *Computers and Geotechnics* 35:286-291, DOI: 10.1016/j.compgeo.2007.09.004

Kelesoglu MK (2016) The evaluation of three-dimensional effects on slope stability by the strength reduction method. *KSCE Journal of Civil Engineering* 20(1):229-242, DOI: 10.1007/s12205-015-0686-4

Krabbenhoft K, Lyamin AV (2015) Strength reduction finite-element limit analysis. *Géotechnique Letters* 5:250-253, DOI: 10.1680/jgele.15.00110

Leij FJ, Alves WJ, van Genuchten MT (1996) The UNSODA - Unsaturated soil hydraulic database, user's manual, version 1.0. National Risk Management Research Laboratory, Office of Research and Development, U.S. Environmental Protection Agency, Cincinnati, OH, USA

Leong EC, Rahardjo H, Tang SK (2003) Characterisation and engineering properties of Singapore residual soils. In: Characterisation and engineering properties of natural soils. A.A. Balkema, Leiden, The Netherlands, 1279-1304

Li L, Chu X (2019) Failure mechanism and factor of safety for spatially variable undrained soil slope. *Advances in Civil Engineering* 2019:8575439, DOI: 10.1155/2019/8575439

Li AJ, Fatty A, Yang IT (2020a) Use of evolutionary computation to improve rock slope back analysis. *Applied Sciences* 10:2012, DOI: 10.3390/app10062012

Li AJ, Jagne A, Lin HD, Huang FK (2020b) Investigation of slurry supported trench stability under seismic condition in purely cohesive soils. *Journal of GeoEngineering* 15:195-203, DOI: 10.6310/jog.202012_15(4).3

Li AJ, Merifield RS, Lyamin AV (2010) Three-dimensional stability charts for slopes based on limit analysis methods. *Canadian Geotechnical Journal* 47:1316-1334, DOI: 10.1139/t10-030

Li AJ, Qian Z, Jiang J-C, Lyamin AV (2019) Seismic slope stability evaluation considering rock mass disturbance varying in the slope. *KSCE Journal of Civil Engineering* 23(3):1043-1054, DOI: 10.1007/s12205-019-0963-8

Lim K, Li AJ, Schmid A, Lyamin AV (2017) Slope-stability assessments using finite-element limit-analysis methods. *Internation Journal of Geomechanics* 17:06016017, DOI: 10.1061/(ASCE)GM.1943-5622.0000715

Lin H, Chen J (2017) Back analysis method of homogeneous slope at critical state. *KSCE Journal of Civil Engineering* 21(3):670-675,

DOI: 10.1007/s12205-016-0400-1
Lin HD, Jiang YS, Wang CC, Chen HY (2016) Assessment of apparent cohesion of unsaturated lateritic soil using an unconfined compression test. Advances in civil, environmental and materials research (ACEM16), August 28-September 1, Jeju, Korea
Lin HD, Wang WC, Li AJ (2020) Investigation of dilatancy angle effects on slope stability using the 3D finite element method strength reduction technique. *Computers and Geotechnics* 118:103295, DOI: 10.1016/j.compgeo.2019.103295
Lu N, Griffiths DV (2004) Profiles of steady-state suction stress in unsaturated soils. *Journal of Geotechnical and Geoenvironmental Engineering* 130:1063-1076, DOI: 10.1061/(ASCE)1090-0241(2004)130:10(1063)
Lyamin AV, Sloan SW (2002a) Lower bound limit analysis using non-linear programming. *International Journal for Numerical Methods in Engineering* 55:573-611, DOI: 10.1002/nme.511
Lyamin AV, Sloan SW (2002b) Upper bound limit analysis using linear finite elements and non-linear programming. *International Journal for Numerical and Analytical Methods in Geomechanics* 26:181-216, DOI: 10.1002/nag.198
Michalowski RL (2002) Stability charts for uniform slopes. *Journal of Geotechnical and Geoenvironmental Engineering* 128:351-355, DOI: 10.1061/(ASCE)1090-0241(2002)128:4(351)
Ng CWW, Shi Q (1998) Influence of rainfall intensity and duration on slope stability in unsaturated soils. *Quarterly Journal of Engineering Geology* 31:105-113, DOI: 10.1144/GSL.QJEG.1998.031.P2.04
Ng CWW, Zhou C, Yuan Q, Xu J (2013) Resilient modulus of unsaturated subgrade soil: Experimental and theoretical investigations. *Canadian Geotechnical Journal* 50:223-232, DOI: 10.1139/cgj-2012-0052
Nguyen TS, Likitlersuang S, Jotisankasa A (2020) Stability analysis of vegetated residual soil slope in Thailand under rainfall conditions. *Environmental Geotechnics* 7:338-349, DOI: 10.1680/jenge.17.00025
Nishimura T, Toyota H, Vanapalli S, Oh W (2008) The shear strength behavior of a silty soil in the residual zone of unsaturation. Proceedings of the 12th international conference of international association for computer methods and advances in geomechanics (IACMAG), October 1-6, Goa, India
Oberhollenzer S, Tschuchnigg F, Schweiger HF (2018) Finite element analyses of slope stability problems using non-associated plasticity. *Journal of Rock Mechanics and Geotechnical Engineering* 10:1091-1101, DOI: 10.1016/j.jrmge.2018.09.002
Oguchi T, Katsube K, Lin Zh, Chen YG (2011) Characteristic slope angle of V-shaped valleys in humid steep mountains with frequent slope failure. *Geomorphometry* 2011
Oh S, Lu N (2014) Slope stability analysis under unsaturated conditions: Case studies of rainfall-induced failure of cut slopes. *Engineering Geology* 184, DOI: 10.1016/j.enggeo.2014.11.007
Oloo YS, Fredlund DG, Gan JKM (1997) Bearing capacity of unpaved roads. *Canadian Geotechnical Journal* 34:398-407, DOI: 10.1139/cgj-34-3-398
Optum (2020) Optum G2 2020. Optum, Retrieved May 5, 2021, https://optumce.com/products/optumg2/
Pang Zh, Gu D (2020) Effects of strength non-homogeneity and non-saturation on stability of a 3D slope. *Journal of GeoEngineering* 15:183-193, DOI: 10.6310/jog.202012_15(4).2
Pradhan SP, Siddique T (2020) Stability assessment of landslide-prone road cut rock slopes in Himalayan terrain: A finite element method based approach. *Journal of Rock Mechanics and Geotechnical Engineering* 12:59-73, DOI: 10.1016/j.jrmge.2018.12.018
Qi Sh, Vanapalli SK (2015) Hydro-mechanical coupling effect on surficial layer stability of unsaturated expansive soil slopes. *Computers and Geotechnics* 70:68-82, DOI: 10.1016/j.compgeo.2015.07.006
Rabczuk T, Belytschko T (2004) Cracking particles: A simplified meshfree method for arbitrary evolving cracks. *International Journal for Numerical Methods in Engineering* 61:2316-2343, DOI: 10.1002/nme.1151
Rabczuk T, Belytschko T (2007) A three-dimensional large deformation meshfree method for arbitrary evolving cracks. *Computer Methods in Applied Mechanics and Engineering* 196:2777-2799, DOI: 10.1016/j.cma.2006.06.020
Rabczuk T, Ren H, Zhuang X (2019) A nonlocal operator method for partial differential equations with application to electromagnetic waveguide problem. *Computers, Materials and Continua* 59:31-55, DOI: 10.32604/cmc.2019.04567
Rabczuk T, Zi G, Bordas S, Nguyen-Xuan H (2010) A simple and robust three-dimensional cracking-particle method without enrichment. *Computer Methods in Applied Mechanics and Engineering* 199:2437-2455, DOI: 10.1016/j.cma.2010.03.031
Rahardjo H, Lim TT, Chang MF, Fredlund DG (1995) Shear-strength characteristics of a residual soil. *Canadian Geotechnical Journal* 32:60-77, DOI: 10.1139/t95-005
Rahardjo H, Ong TH, Rezaur RB, Leong EC (2007) Factors controlling instability of homogeneous soil slopes under rainfall. *Journal of Geotechnical and Geoenvironmental Engineering* 133:1532-1543, DOI: 10.1061/(ASCE)1090-0241(2007)133:12(1532)
Rahim MSM (2016) Hydro-mechanical behaviour of a residual soil slope in Malaysia. PhD Thesis, Durham University, Durham, UK
Rassam DW, Williams DJ (1999) A relationship describing the shear strength of unsaturated soils. *Canadian Geotechnical Journal* 36:363-368, DOI: 10.1139/t98-102
Ren H, Zhuang X, Cai Y, Rabczuk T (2016) Dual-horizon peridynamics. *International Journal for Numerical Methods in Engineering* 108:1451-1476, DOI: 10.1002/nme.5257
Rocscience (2019) RS2 2019. Rocscience, Retrieved April 26, 2021, https://www.rocscience. com/software/rs2
Shin H, Kim YT, Park DK (2013) Development of rainfall hazard envelope for unsaturated infinite slope. *KSCE Journal of Civil Engineering* 17(3):351-356, DOI: 10.1007/s12205-013-1626-9
Sloan SW (2013) Geotechnical stability analysis. *Géotechnique* 63:531-571, DOI: 10.1680/geot.12.RL.001
Tian DF, Zheng H, Liu DF (2017) A 2D integrated FEM model for surface water–groundwater flow of slopes under rainfall condition. *Landslides* 14:577-593, DOI: 10.1007/s10346-016-0716-4
Timoshenko S, Goodier JN (1951) Theory of elasticity. McGraw Hill, New York, NY, USA
Tohari A, Nishigaki M, Komatsu M (2007) Laboratory rainfall-induced slope failure with moisture content measurement. *Journal of Geotechnical and Geoenvironmental Engineering* 133:575-587, DOI: 10.1061/(ASCE)1090-0241(2007)133:5(575)
Toll DG, Rahardjo H, Leong EC (1999) Landslides in Singapore. Proceedings of the 2nd international conference on landslides, slope stability and the safety of infra-structures, July 27-28, Singapore, 269-276
Tsaparas I, Rahardjo H, Toll DG, Leong EC (2002) Controlling parameters for rainfall-induced landslides. *Computers and Geotechnics* 29:1-27, DOI: 10.1016/S0266-352X(01)00019-2
Tschuchnigg F, Schweiger HF, Sloan SW (2015a) Slope stability analysis by means of finite element limit analysis and finite element strength reduction techniques. Part I: Numerical studies considering non-associated plasticity. *Computers and Geotechnics* 70:169-177,

DOI: 10.1016/j.compgeo.2015.06.018

Tschuchnigg F, Schweiger HF, Sloan SW, Lyamin AV, Raissakis I (2015b) Comparison of finite-element limit analysis and strength reduction techniques. *Géotechnique* 65:249-257, DOI: 10.1680/geot.14.P.022

Vanapalli SK, Fredlund DG, Pufahl DE, Clifton AW (1996) Model for the prediction of shear strength with respect to soil suction. *Canadian Geotechnical Journal* 33:379-392, DOI: 10.1139/t96-060

Vereecken H, Weynants M, Javaux M, Pachepsky Y, Schaap MG, van Genuchten MT (2010) Using pedotransfer functions to estimate the van genuchten–mualem soil hydraulic properties: A review. *Vadose Zone Journal* 9:795-820, DOI: 10.2136/vzj2010.0045

Yang KH, Nguyen ThS, Rahardjo H, Lin DG (2021) Deformation characteristics of unstable shallow slopes triggered by rainfall infiltration. *Bulletin of Engineering Geology and the Environment* 80:317-344, DOI: 10.1007/s10064-020-01942-4

Yang KH, Uzuoka R, Thuo JN, Lin GL, Nakai Y (2017) Coupled hydro-mechanical analysis of two unstable unsaturated slopes subject to rainfall infiltration. *Engineering Geology* 216:13-30, DOI: 10.1016/j.enggeo.2016.11.006

Yao Y, Zheng J, Zhang J, Peng J, Li J (2018) Model for predicting resilient modulus of unsaturated subgrade soils in South China. *KSCE Journal of Civil Engineering* 22(6):2089-2098, DOI: 10.1007/s12205-018-1703-1

Zhang LL, Fredlund DG, Fredlund MD, Ward WG (2014) Modeling the unsaturated soil zone in slope stability analysis. *Canadian Geotechnical Journal* 51:1384-1398, DOI: 10.1139/cgj-2013-0394

Zhou H, Zheng G, Yin X, Jia R, Yang X (2018) The bearing capacity and failure mechanism of a vertically loaded strip footing placed on the top of slopes. *Computers and Geotechnics* 94:12-21, DOI: 10.1016/j.compgeo.2017.08.009